ACS APPLIED NANO MATERIALS

www.acsanm.org

Letter

Optical Properties of Stanene-like Nanosheets on $Al_2O_3(0001)$: Implications for Xene Photonics

Carlo Grazianetti, Eleonora Bonaventura, Christian Martella, Alessandro Molle,* and Stefano Lupi*

Cite This: *ACS Appl. Nano Mater.* 2021, 4, 2351−2356

Read Online

ACCESS | Metrics & More | Article Recommendations | Supporting Information

ABSTRACT: Stanene is one of the most intriguing two-dimensional (2D) materials because of its nontrivial topological properties. Here, the optical properties from THz to UV of molecular beam deposited tin nanosheets on $Al_2O_3(0001)$ are reported. The experimental absorption coefficient cannot be described in terms of metallic tin or tin oxides. Nonetheless, a similar optical behavior was predicted by theory for freestanding stanene, thus suggesting the formation of the 2D tin nanosheets with stanene-like properties. These findings show that 2D tin bears appealing optical properties in a broad range of the electromagnetic spectrum, thus paving the way to Xenes-based nanophotonics.

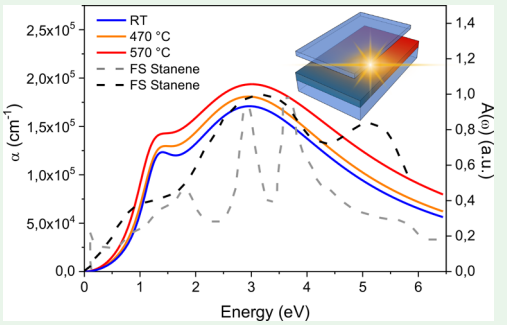

KEYWORDS: *stanene, Xenes, molecular beam epitaxy, optical spectroscopy, absorption coefficient*

Recent years have witnessed the rise of two-dimensional (2D) materials after the astonishing and unprecedented properties of graphene. In this framework, the revolution started by graphene shed light on a new world where the third dimension is dramatically reduced below the nanometer scale. A wealth of 2D materials, including Xenes,[1] transition metal (TM) dichalcogenides,[2] TM carbides and nitrides,[3] and TM oxides,[4] are today probably among the most flourishing topic related to condensed matter physics. In particular, the different electronic properties of 2D materials look promising to cover the electromagnetic spectrum, thus paving the way to unprecedented applications in photonics.[5−7] However, most importantly and complementary to the 2D downscaling, the recent discoveries about topological insulators focused attention on a renewed interest in those materials already studied in the past. One of the most intriguing examples in this framework is represented by α-Sn whose topological properties have been disclosed only recently.[8,9] Following the synthesis of silicene on $Al_2O_3(0001)$[10] and aiming at investigating the properties of heavy Xenes like stanene on the same substrate,[11] here we report on the unconventional optical properties of 2D tin nanosheets in the photon range from THz to UV. On one hand, the rush in synthesizing heavy Xenes like stanene on nonconductive substrates is highly demanded to exploit their quantum spin Hall (QSH) insulator state because of the large spin−orbit coupling (SOC). Indeed, the heavier mass of tin in comparison to those of the elements above, *e.g.*, silicon, makes stanene appealing from the topological point of view, thus representing a suitable single-element candidate for the long-sought 2D topological insulator. Indeed, the SOC converts a honeycomb lattice from an ideal semimetal to a QSH insulator. On the other hand, the revisited properties of α-Sn demonstrate that unexpected behaviors could be hints of novel states of matter as well, *e.g.*, Ising superconductivity in few-layer stanene.[12] Therefore, in the present study, aiming at synthesizing stanene on the transparent substrate $Al_2O_3(0001)$, so-called C-plane sapphire, we report on an unexpected and novel optical behavior of 2D tin films with spectral features demonstrating stanene-like properties differing from conventional metallic and oxide tin phases reported to date. These outcomes on the first-time reported synthesis of stanene-like nanosheets on a transparent substrate pave the way to photonics applications in Xenes-based devices operating in a broad range of the electromagnetic spectrum.

In order to access the 2D properties of tin on the $Al_2O_3(0001)$ substrate grown by molecular beam epitaxy (MBE) deposition, first the chemical environment was scrutinized by X-ray photoelectron spectroscopy (XPS), and subsequently the optical properties were unraveled by transmittance and reflectance measurements. The starting growth nominal thickness considered is 0.5 nm, whereas the growth temperature (T_G) has been varied among room temperature (RT), 470, and 570 °C (see Methods and Supporting Information Table S1). The chemical interaction between tin and $Al_2O_3(0001)$ is disclosed through *in situ* XPS. The XPS analysis performed on the tin films deposited on

Received: December 2, 2020
Accepted: January 24, 2021
Published: March 10, 2021

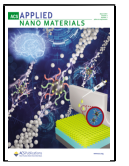

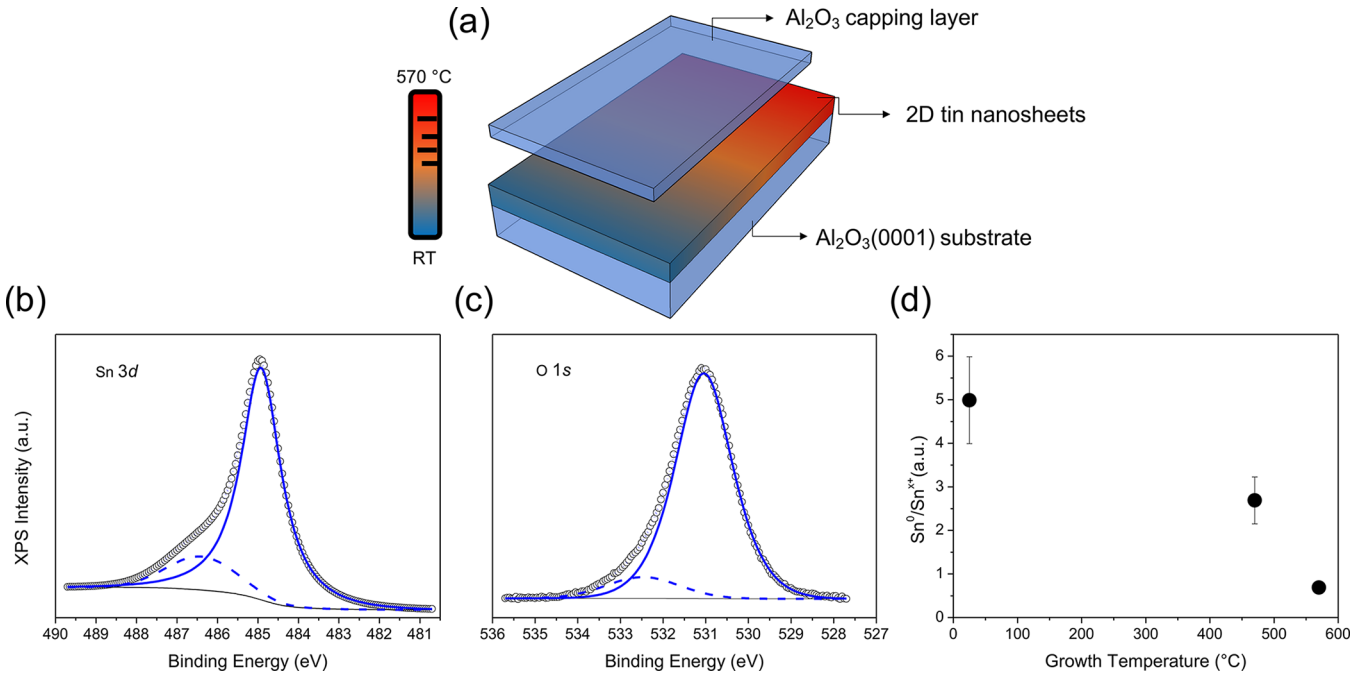

Figure 1. (a) Scheme of the samples from top to bottom: amorphous Al_2O_3 capping layer grown by codeposition, 2D tin nanosheets grown by MBE (T_G from RT to 570 °C), and Al_2O_3(0001) substrate. (b) XPS Sn $3d_{5/2}$ core level of 0.5 nm tin grown at RT on Al_2O_3(0001) showing Sn^0 (blue line) and Sn^{x+} (blue dashed line) components related to the elemental and oxidized states of tin along with raw data (open circles) and full fit (blue dotted line). (c) XPS O 1s core level showing two components related to the substrate (low-BE, blue line) and to the hydroxyl groups (high-BE, blue dashed line). (d) Ratio Sn^0/Sn^{x+} of the three samples grown at different substrate temperature (RT, 470, and 570 °C). All the XPS spectra are recorded before Al_2O_3 capping layer.

Al_2O_3(0001) substrates accounted for C 1s (used as reference for charging effects),[10] Al 2p, O 1s, and Sn 3d (hereafter, only the Sn $3d_{5/2}$ will be considered) core levels. Figure 1 reports the representative XPS spectra before the Al_2O_3 capping necessary for *ex situ* investigation (see Methods and Figure 1a for a schematic sketch of the samples), just after the tin deposition, thus preventing oxidation. Independently of the substrate temperature (at the same tin thickness), all the samples scrutinized showed two components of the Sn $3d_{5/2}$ core level (hereafter Sn^0 and Sn^{x+}), where the one at higher binding energy (BE) can be likely related to an oxidation state (Sn^{x+}). Figure 1b reports on the deposition of 0.5 nm at RT showing two components: Sn^0 narrower at lower BE [BE = 484.93 eV and full-width half-maximum (fwhm) = 1.18 eV] and Sn^{x+} broader at higher BE (BE = 486.4 eV and fwhm = 2 eV). It is interesting to note that even at RT tin undergoes oxidation, as other metals on the same substrate.[13−15] The difference in BE between the metallic and the oxidized components is about 1.5 eV in all the 0.5 nm-thick nanosheet samples (RT to 570 °C), whereas the ratio between the metal and oxide components is not (see below). From the literature, the BE of the elemental component Sn^0 is placed on average at 484.98 eV and the SnO and SnO_2 oxidation states are at 486.16 and 486.79 eV, respectively.[16−18] Moreover, on the R-plane sapphire, *i.e.*, Al_2O_3(−1012), the Sn $3d_{5/2}$ core level was observed at BE = 486.2 eV with a SnO stoichiometry.[19] Therefore, the BE shift observed can be likely related to an intermediate oxidation state between SnO and SnO_2 in all the considered samples (hence, $2 < x < 4$). On the other hand, an uncertainty in the determination of the oxidation state is still present because of the final effect states of photoemission related to small metallic particles on insulating substrates, namely, a Coulomb shift superimposed to the chemical shift, as reported for vanadium deposition on Al_2O_3(0001).[14] Additional experiments will be necessary to unravel the precise stoichiometry of such an oxide. However, the origin of this oxidation can be likely related to the interaction between tin and oxygen atoms of the Al_2O_3(0001), even if the surface is Al-terminated,[20] as confirmed by the shift at higher BE of the O 1s core levels, showing two components (Figure 1c) even on the pristine sample (data not shown), whereas the Al 2p core level is unaffected by tin deposition (see Supporting Information Figure S1), either BE or fwhm. The surface oxygens can then be related to the presence of adsorbed hydroxyl group (−OH) on the surface of Al_2O_3(0001) as demonstrated by ion-scattering experiments (see also the Supporting Information).[21] When the T_G is increased from RT to 570 °C, the fwhm values of the two tin components (Sn^0 and Sn^{x+}) are as those of Figure 1b (1.2 and 2 eV, respectively), but the ratio between the metallic and oxide components Sn^0/Sn^{x+} drops from 4.99 to 0.69, thus evidencing an increased interaction between tin and the substrate. The overall trend of the ratio between metal and oxide decreases with increasing growth temperature from RT to 570 °C, as reported in Figure 1d.

Reflectance $R(\omega)$ and transmittance $T(\omega)$ optical measurements were performed in the range from THz to UV (0.01−6.45 eV or 80−52000 cm^{-1}) and are reported in Figure S2 of the Supporting Information. In particular, transmittance measurements have been performed in the substrate transparency region, *i.e.*, below 0.035 eV and above 0.12 eV, while reflectance measurements have been collected in the range from 0.035 to 0.12 eV because of the strong IR phonon absorption of the Al_2O_3(0001) substrate.[22] In the FIR region (0.01−0.035 eV in transmittance and 0.025−0.17 eV in reflectance), no optical signatures of the tin nanosheets can be

https://dx.doi.org/10.1021/acsanm.0c03221
ACS Appl. Nano Mater. 2021, 4, 2351−2356

observed, thus suggesting an optical bandgap fairly compatible with theoretical prediction for stanene.[11] Indeed, a gap as large as 0.25 eV opens after SOC is turned on in *ab initio* calculations, indicative of the nontrivial topological feature of stanene/Al_2O_3(0001). Conversely, in the MIR-Vis-UV photon energy range the tin nanosheets show an optical response different from the substrate (from 0.17 to 6.45 eV) as reported in Supporting Information Figures S2−S4. Figure 2 reports on

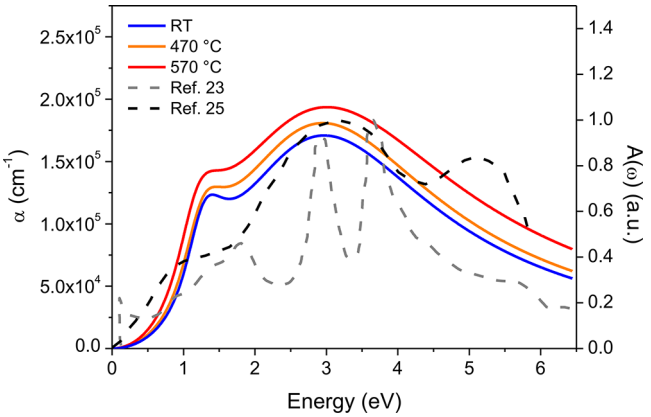

Figure 2. Absorption coefficients $\alpha(\omega)$ of 0.5 nm-thick samples grown at RT (blue), 470 °C (orange), and 570 °C (red). The theoretical absorbance $A(\omega)$ of freestanding stanene (black and gray dashed lines) is reported for comparison (data from refs 23 and 25).

the absorption coefficients of the 0.5 nm-thick films deposited at increasing T_G (from RT to 570 °C). The absorption coefficient $\alpha(\omega)$ is extracted from the multilayer model by considering both the measured $T(\omega)$ and $R(\omega)$ via the imaginary part of the refractive index: $\alpha(\omega) = 2\omega k(\omega)/c$, where $k(\omega)$ is the imaginary part of the refractive index $\tilde{n}$ and c is the speed of light. The amorphous capping layer, because of its small thickness and intrinsic transparency, does not affect the optical properties of tin nanosheets on Al_2O_3(0001) (see Supporting Information Figure S1); moreover, $\alpha(\omega)$ has been obtained by considering the actual complex refractive index of Al_2O_3(0001) as determined from its absolute transmittance and reflectance measured for a bare substrate coming from the same batch (see Supporting Information Figures S3 and S4). The optical response is shown to be nearly T_G-independent for the three scrutinized samples (Figure 2), despite the different ratio between the metallic and oxidized components (see Figure 1d). Indeed, their absorption coefficients show a quite similar shape characterized by two broad peaks centered at nearly 1.25 and 3 eV. In order to assign those absorption features, in the same figure we compare the experimental absorption spectra (left scale) with that calculated for freestanding stanene (right scale) reported by Matthes *et al.* (gray dashed line in Figure 2).[23] The theoretical absorbance spectrum shows a first peak around 1.8 eV as a consequence of 2D saddle points in the $\pi-\pi^*$ interband structure of stanene located at the six M points at the Brillouin zone boundary. The higher-energy peaks near 3.1 and 4.0 eV are instead related to $\sigma-\sigma^*$ transitions mainly at the Γ point of the 2D Brillouin zone.[23,24] It is possible to notice that the experimental absorption feature of tin nanosheets at nearly 1.25 eV is red-shifted with respect to the theoretical one (at about 1.8 eV) of freestanding stanene, while the theoretical two-peak structure (at 3.1 and 4 eV) merges in a single broad feature (located around 3 eV) in the experimental data, likely because of interaction with Al_2O_3(0001) substrate, as already demonstrated for silicene.[10] The experimental absorption coefficients in the low-energy part of the photon range, *i.e.*, $\alpha(\omega \rightarrow 0)$, show a vanishing intensity toward the THz region [where $\alpha(\omega) = 0$ as mentioned before] without a sharp absorption edge as shown in the theoretical calculation.[23] However, it is important to observe that the reported calculation has been performed at zero temperature, and hence, the expected gap should be smoothed at finite temperature. On the other hand, John *et al.* theoretically separated the contribution to absorbance coming from parallel and normal (to the basal plane) polarized incident light for stanene and other Xenes.[25] In Figure 2 their calculated absorbance $A(\omega)$ (black dashed line, parallel polarization like in the present experiments) shows even better agreement with the experimental data. Indeed, the broad theoretical peak centered at 3.27 eV (due to transitions among parallel bands formed along the K−Γ direction by p_z and σ^* orbitals) can be easily compared to the experimental broad feature centered around 3 eV. Conversely, the next peak at 5.21 eV (electronic transition from p_x hybridized orbital and π^*) is not experimentally observed, being probably confused in the high-energy experimental absorption tail. Finally, absorption starts at 1.27 eV photon

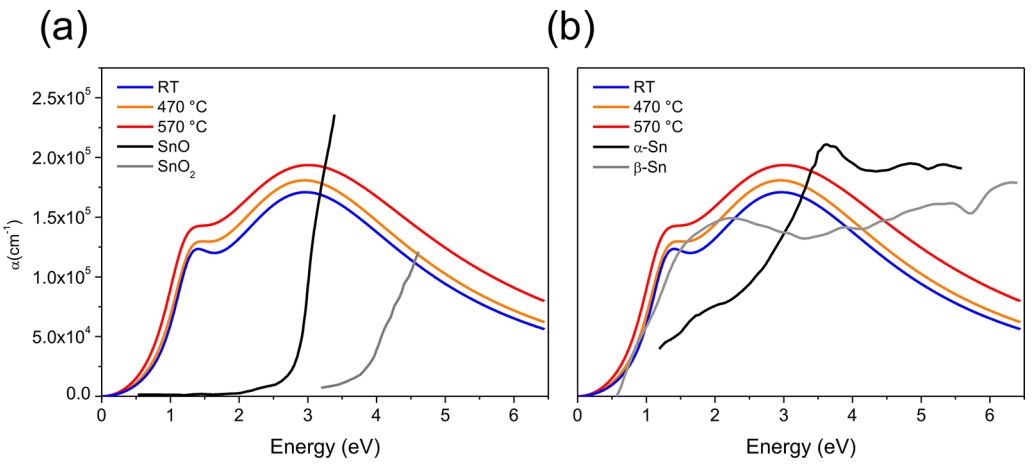

Figure 3. (a) Comparison between the absorption coefficients of Figure 2 and those of SnO (black) and SnO_2 (gray) (data from refs 27 and 28). (b) Comparison between the absorption coefficients of Figure 2 and those of α-Sn (black) and β-Sn (gray) (data from refs 29 and 30).

https://dx.doi.org/10.1021/acsanm.0c03221
ACS Appl. Nano Mater. 2021, 4, 2351−2356

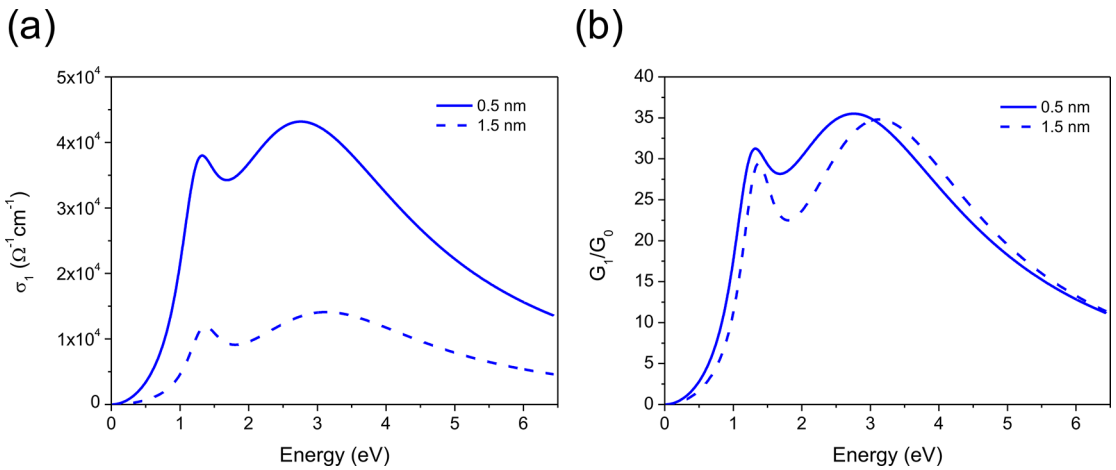

Figure 4. (a) Real part of the optical conductivity σ_1 of 0.5 (blue) and 1.5 nm (blue dashed) 2D tin nanosheets. (b) Real part of the optical conductance normalized to the universal optical conductance G_1/G_0 of 0.5 (blue) and 1.5 (blue dashed) nm-thick 2D tin nanosheets grown at RT.

energies with a small hump (and not a sharp peak) because stanene bands do not become as flat as the other Xenes (graphene, silicene, and germanene), and hence, the van Hove singularity related to $\pi-\pi^*$ interband transition is broadened, in good agreement with the experimental feature placed at 1.25 eV. Finally, the experimental absorption coefficients of Figure 2 show also similar features reported in the theoretical absorbance spectrum of fully hydrogenated stanene, *i.e.*, stanane, which is characterized by a larger bandgap opening at the Γ point of the Brillouin zone (1.22 eV) but still keeps the $\pi-\pi^*$ interband transition around 3 eV.[26]

The comparison between experimental data and theoretical calculations suggests that, when scaled down to 2D regime, 2D tin nanosheets on $Al_2O_3(0001)$ are endowed with stanene-like properties. In order to further support this finding, we compare in Figure 3 the observed optical response of tin nanosheets with the absorption coming from known elemental allotropes of tin and various tin oxides. Figure 3a presents the absorption coefficients of 0.5 nm-thick 2D tin nanosheets from RT to 570 °C with those of SnO and SnO_2.[27,28] Both oxides are electric insulators and present a large optical gap, around 3 eV for SnO and 4 eV for SnO_2. Although the photon energy range scrutinized is different, an overall behavior can be clearly observed because of the lack of a large gap in the $\alpha(\omega)$ curves of the 2D tin nanosheets. By and large, the optical contribution of the tin oxides to the observed spectra can potentially be taken into account only for $\hbar\omega > 3$ eV, thus ruling out an optical response related to the oxide component below this threshold. On the other hand, a similar comparison with the α- and β-Sn phases,[29,30] namely, gray and white tin (the former is a zero bandgap semiconductor with cubic diamond structure, whereas the latter is a metal with body-centered tetragonal structure), is reported in Figure 3b. The absorption coefficient of the 2D tin nanosheets does not resemble either α- and β-Sn absorption coefficients or a linear combination of both, thus suggesting an unprecedented phase for tin in this growth regime. Therefore, both results in Figure 3a,b further suggest that 2D tin films on $Al_2O_3(0001)$ show stanene-like properties.

In light of the recent discoveries about few-layer stanene and α-Sn,[8,9,12] it is interesting to explore a thicker growth regime. Figure 4 shows the comparison between 0.5 and 1.5 nm-thick samples grown at RT. The real part of the optical conductivity $\sigma_1 = \alpha(\omega)nc/4\pi$, where $\sigma(\omega) = \sigma_1 + i\sigma_2$ (α is the absorption coefficient, and n is the refractive index), is reported in Figure 4a. An intriguing trend is observed when increasing the thickness of the 2D tin nanosheets from 0.5 to 1.5 nm, showing an inverse behavior of σ_1 intensity versus the film thickness. Remarkably the optical conductivity of the 1.5 nm-thick nanosheet displays the same optical spectrum characterized by stanene-like features of the thinnest sample (broad peaks at 1.25 and 3 eV are clearly observed). The introduction of the thickness parameter, *i.e.*, a dimensional parameter, might suggest a dimensional crossover as already observed for silicon on the same substrate.[10] However, unlike the silicon case we do not observe changes in the optical conductivity spectrum when increasing thickness from 0.5 to 1.5 nm. Further comparison can be carried out by considering the optical conductance, G_1. When considering the optical conductance $G_1 = \sigma_1 d$ where d is the film thickness in terms of the universal optical conductance $G_0 = 6.08 \times 10^{-5}\ \Omega^{-1}$, it is possible to observe that the low-energy spectral features of 0.5 and 1.5 nm G_1/G_0 spectra nearly superimpose, whereas the high-energy feature is slightly blue-shifted in the 1.5 nm G_1/G_0 spectrum compared to the 0.5 nm spectrum (Figure 4b). This comparison based on a dimensional renormalization thus evidences a thickness-dependent behavior of the optical response intensity of 2D tin nanosheets, whereas the stanene-like optical fingerprints are nearly conserved (see Figure 2), suggesting the presence of a single active stanene-like layer in both samples, which is likely superimposed to an optically inert layer in the 1.5 nm-thick sample.

In summary, 2D tin nanosheets on $Al_2O_3(0001)$ substrate were grown by MBE at different deposition temperature from RT to 570 °C. Partial oxidation occurring in the tin nanosheets can be explained by the unavoidable interaction between tin and hydroxyl groups naturally present on the $Al_2O_3(0001)$ surface. The optical behavior of the tin films at the 2D limit is very similar to each other and strongly differs from those of common tin oxide (SnO and SnO_2) and from those of conventional elemental tin phases (α- and β-Sn). Most importantly, absorption spectra show characteristic signatures that closely resemble those of freestanding stanene endowed with SOC-induced bandgap as well as absorption peaks due to electronic interband transitions along high-symmetry directions of the Brillouin zone. The nontrivial nature of 2D tin nanosheets on $Al_2O_3(0001)$ is further corroborated by an

https://dx.doi.org/10.1021/acsanm.0c03221
ACS Appl. Nano Mater. 2021, 4, 2351−2356

interesting thickness-dependent optical response characterized by a decrease of the optical conductivity intensity for thicker films. However, when dimensional renormalization is taken into account through an optical conductance comparison, the optical behavior turns out to be almost identical to the stanene-like spectrum of the thinnest nanosheet throughout the broad electromagnetic spectrum (from THz to UV) here scrutinized. Accessing the optical properties of dimensionally reduced tin nanosheets allowed disclosing an optical behavior that cannot be related to conventional tin, thus paving the way to optoelectronic and photonic engineering of novel and high-performance optoelectronic devices, mostly active in the visible region.

METHODS

MBE Growth and Encapsulation. One-side polished $Al_2O_3(0001)$ substrates were degassed in ultrahigh vacuum (base pressure 10^{-10} mbar) at ∼250 °C for a few hours before tin deposition. Tin growth onto substrates was performed by MBE using a k-cell evaporator after calibration of flux rate through microbalance. Three different samples were grown at variable temperature ranging from RT (∼25 °C) to 570 °C. Temperature readings were crosschecked by pyrometer-based calibration of the thermocouple attached under the sample holder. The tin films were subsequently protected using an *in situ* grown transparent capping layer made of aluminum oxide (∼5 nm) as for other Xenes like silicene and blue phosphorene. In detail, the amorphous 5 nm-thick Al_2O_3 capping layer was grown *in situ* through reactive codeposition of a pure aluminum beam in a molecular oxygen atmosphere (partial pressure 10^{-6} mbar). Hence, the overall stacking from top to bottom is Al_2O_3/Sn/$Al_2O_3(0001)$, similar to that used for silicene.[10]

XPS Characterization. Before and after the tin and Al_2O_3 depositions, the chemical status was monitored by means of *in situ* nonmonochromatized XPS ($h\nu$ = 1253.6 eV). Surface sensitive measurements were performed at a takeoff angle of 37° between the sample surface and the hemispherical electron analyzer.

Optical Spectroscopy. The macroscopic optical properties, *i.e.*, absolute transmittance $T(\omega)$ and reflectance $R(\omega)$, were then measured at RT from THz to UV (0.01−6.45 eV or 80−52000 cm^{-1}) on several thin films from 0.5 to 1.5 nm, and the microscopic optical properties were extracted using a multilayer model with RefFIT.[31] Measurements were recorded even at low-temperature (78 K) with no differences with those at RT. In particular, the following spectral regions were scrutinized: 0.01−0.031 eV (80−250 cm^{-1}) (THz in transmission, vacuum), 0.031−0.18 eV (250−1500 cm^{-1}) (IR reflectance, vacuum), and 0.17−6.45 eV (1400−52000 cm^{-1}) (transmittance from IR to UV, vacuum from 1400 to 8000 cm^{-1}, and in atmosphere from 8000 to 52000 cm^{-1}).

ASSOCIATED CONTENT

Supporting Information

The Supporting Information is available free of charge at https://pubs.acs.org/doi/10.1021/acsanm.0c03221.

Supporting text on the hydroxyl groups on the $Al_2O_3(0001)$ surface, additional evidence on the tin nanosheets thickness (Table S1), Al 2p and Sn 3d core levels data (Figure S1), reflectance $R(\omega)$ and transmittance $T(\omega)$ data (Figure S2), real and imaginary parts of the refraction index of the $Al_2O_3(0001)$ substrate (Figure S3), and absorption coefficient $\alpha(\omega)$ of the $Al_2O_3(0001)$ substrate (Figure S4) (PDF)

AUTHOR INFORMATION

Corresponding Authors

Alessandro Molle − *CNR-IMM Unit of Agrate Brianza, Agrate Brianza I-20864, Italy*; orcid.org/0000-0002-3860-4120; Email: alessandro.molle@mdm.imm.cnr.it

Stefano Lupi − *CNR-IOM Dipartimento di Fisica, Sapienza Università di Roma, Roma I-00185, Italy*; Email: stefano.lupi@roma1.infn.it

Authors

Carlo Grazianetti − *CNR-IMM Unit of Agrate Brianza, Agrate Brianza I-20864, Italy*; orcid.org/0000-0003-0060-9804

Eleonora Bonaventura − *CNR-IMM Unit of Agrate Brianza, Agrate Brianza I-20864, Italy*

Christian Martella − *CNR-IMM Unit of Agrate Brianza, Agrate Brianza I-20864, Italy*; orcid.org/0000-0003-1811-165X

Complete contact information is available at: https://pubs.acs.org/10.1021/acsanm.0c03221

Notes

The authors declare no competing financial interest.

ACKNOWLEDGMENTS

A.M. acknowledges EU funding from the H2020 research and innovation programme under the ERC-COG 2017 Grant No. 772261 "XFab". S.L. acknowledges the financial support of the Bilateral Cooperation Agreement between Italy and China of the Italian Ministry of Foreign Affairs and of the International Cooperation (MAECI) in the framework of the project of major relevance N. PGR00772. The authors also acknowledge Mario Alia (CNR-IMM) for technical support.

REFERENCES

(1) Grazianetti, C.; Martella, C.; Molle, A. The Xenes Generations: A Taxonomy of Epitaxial Single-Element 2D Materials. *Phys. Status Solidi RRL* **2020**, *14* (2), 1900439.

(2) Manzeli, S.; Ovchinnikov, D.; Pasquier, D.; Yazyev, O. V.; Kis, A. 2D Transition Metal Dichalcogenides. *Nature Reviews Materials* **2017**, *2*, 17033.

(3) Khazaei, M.; Arai, M.; Sasaki, T.; Chung, C. Y.; Venkataramanan, N. S.; Estili, M.; Sakka, Y.; Kawazoe, Y. Novel Electronic and Magnetic Properties of Two-Dimensional Transition Metal Carbides and Nitrides. *Adv. Funct. Mater.* **2013**, *23* (17), 2185−2192.

(4) Yang, T.; Song, T. T.; Callsen, M.; Zhou, J.; Chai, J. W.; Feng, Y. P.; Wang, S. J.; Yang, M. Atomically Thin 2D Transition Metal Oxides: Structural Reconstruction, Interaction with Substrates, and Potential Applications. *Adv. Mater. Interfaces* **2019**, *6* (1), 1801160.

(5) Xia, F.; Wang, H.; Xiao, D.; Dubey, M.; Ramasubramaniam, A. Two-Dimensional Material Nanophotonics. *Nat. Photonics* **2014**, *8* (12), 899−907.

(6) Liu, J.; Xia, F.; Xiao, D.; García de Abajo, F. J.; Sun, D. Semimetals for High-Performance Photodetection. *Nat. Mater.* **2020**, *19* (8), 830−837.

(7) Lupi, S.; Molle, A. Emerging Dirac Materials for THz Plasmonics. *Appl. Mater. Today* **2020**, *20*, 100732.

(8) Barfuss, A.; Dudy, L.; Scholz, M. R.; Roth, H.; Höpfner, P.; Blumenstein, C.; Landolt, G.; Dil, J. H.; Plumb, N. C.; Radovic, M.; Bostwick, A.; Rotenberg, E.; Fleszar, A.; Bihlmayer, G.; Wortmann, D.; Li, G.; Hanke, W.; Claessen, R.; Schäfer, J. Elemental Topological Insulator with Tunable Fermi Level: Strained α -Sn on InSb(001). *Phys. Rev. Lett.* **2013**, *111* (15), 157205.

(9) Xu, C.-Z.; Chan, Y.-H.; Chen, Y.; Chen, P.; Wang, X.; Dejoie, C.; Wong, M.-H.; Hlevyack, J. A.; Ryu, H.; Kee, H.-Y.; Tamura, N.; Chou,

https://dx.doi.org/10.1021/acsanm.0c03221
ACS Appl. Nano Mater. 2021, 4, 2351−2356

M.-Y.; Hussain, Z.; Mo, S.-K.; Chiang, T.-C. Elemental Topological Dirac Semimetal: α -Sn on InSb(111). *Phys. Rev. Lett.* **2017**, *118* (14), 146402.
(10) Grazianetti, C.; De Rosa, S.; Martella, C.; Targa, P.; Codegoni, D.; Gori, P.; Pulci, O.; Molle, A.; Lupi, S. Optical Conductivity of Two-Dimensional Silicon: Evidence of Dirac Electrodynamics. *Nano Lett.* **2018**, *18* (11), 7124−7132.
(11) Wang, H.; Pi, S. T.; Kim, J.; Wang, Z.; Fu, H. H.; Wu, R. Q. Possibility of Realizing Quantum Spin Hall Effect at Room Temperature in Stanene/Al_2O_3(0001). *Phys. Rev. B: Condens. Matter Mater. Phys.* **2016**, *94* (3), No. 035112.
(12) Falson, J.; Xu, Y.; Liao, M.; Zang, Y.; Zhu, K.; Wang, C.; Zhang, Z.; Liu, H.; Duan, W.; He, K.; Liu, H.; Smet, J. H.; Zhang, D.; Xue, Q. K. Type-II Ising Pairing in Few-Layer Stanene. *Science (Washington, DC, U. S.)* **2020**, *367* (6485), 1454−1457.
(13) Niu, C.; Shepherd, K.; Martini, D.; Tong, J.; Kelber, J. A.; Jennison, D. R.; Bogicevic, A. Cu Interactions with α-Al_2O_3(0001): Effects of Surface Hydroxyl Groups versus Dehydroxylation by Ar-Ion Sputtering. *Surf. Sci.* **2000**, *465* (1−2), 163−176.
(14) Biener, J.; Bäumer, M.; Madix, R. J.; Liu, P.; Nelson, E.; Kendelewisz, T.; Brown, G. Growth and Electronic Structure of Vanadium on α-Al_2O_3(0001). *Surf. Sci.* **2000**, *449* (1−3), 50−60.
(15) Kelber, J. A.; Niu, C.; Shepherd, K.; Jennison, D. R.; Bogicevic, A. Copper Wetting of α-Al_2O_3(0001): Theory and Experiment. *Surf. Sci.* **2000**, *446* (1−2), 76−88.
(16) Stranick, M. A.; Moskwa, A. SnO by XPS. *Surf. Sci. Spectra* **1993**, *2* (1), 45−49.
(17) Stranick, M. A.; Moskwa, A. SnO_2 by XPS. *Surf. Sci. Spectra* **1993**, *2* (1), 50−54.
(18) Jie, L.; Chao, X. XPS Examination of Tin Oxide on Float Glass Surface. *J. Non-Cryst. Solids* **1990**, *119* (1), 37−40.
(19) Pan, X. Q.; Fu, L. Tin Oxide Thin Films Grown on the $(\bar{1}012)$ Sapphire Substrate. *J. Electroceram.* **2001**, *7* (1), 35−46.
(20) Eng, P. J.; Trainor, T. P.; Brown, G. E.; Waychunas, G. A.; Newville, M.; Sutton, S. R.; Rivers, M. L. Structure of the Hydrated α-Al_2O_3(0001) Surface. *Science (Washington, DC, U. S.)* **2000**, *288* (5468), 1029−1033.
(21) Ahn, J.; Rabalais, J. W. Composition and Structure of the Al_2O_3{0001}-(1 × 1) Surface. *Surf. Sci.* **1997**, *388* (1−3), 121−131.
(22) Barker, A. S. Infrared Lattice Vibrations and Dielectric Dispersion in Corundum. *Phys. Rev.* **1963**, *132* (4), 1474−1481.
(23) Matthes, L.; Pulci, O.; Bechstedt, F. Optical Properties of Two-Dimensional Honeycomb Crystals Graphene, Silicene, Germanene, and Tinene from First Principles. *New J. Phys.* **2014**, *16* (10), 105007.
(24) Matthes, L.; Pulci, O.; Bechstedt, F. Massive Dirac Quasiparticles in the Optical Absorbance of Graphene, Silicene, Germanene, and Tinene. *J. Phys.: Condens. Matter* **2013**, *25* (39), 395305.
(25) John, R.; Merlin, B. Optical Properties of Graphene, Silicene, Germanene, and Stanene from IR to Far UV − A First Principles Study. *J. Phys. Chem. Solids* **2017**, *110*, 307−315.
(26) Fadaie, M.; Dideban, D.; Gülseren, O. Electronic and Optical Properties of Stanane and Armchair Stanane Nanoribbons. *Appl. Phys. A: Mater. Sci. Process.* **2020**, *126* (6), 460.
(27) Ogo, Y.; Hiramatsu, H.; Nomura, K.; Yanagi, H.; Kamiya, T.; Hirano, M.; Hosono, H. P -Channel Thin-Film Transistor Using p -Type Oxide Semiconductor, SnO. *Appl. Phys. Lett.* **2008**, *93* (3), No. 032113.
(28) Shanthi, E.; Dutta, V.; Banerjee, A.; Chopra, K. L. Electrical and Optical Properties of Undoped and Antimony-Doped Tin Oxide Films. *J. Appl. Phys.* **1980**, *51* (12), 6243−6251.
(29) Takeuchi, K.; Adachi, S. Optical Properties of β-Sn Films. *J. Appl. Phys.* **2009**, *105* (7), No. 073520.
(30) Via, L.; Höchst, H.; Cardona, M. Dielectric Function of α-Sn and Its Temperature Dependence. *Phys. Rev. B: Condens. Matter Mater. Phys.* **1985**, *31* (2), 958−967.
(31) Kuzmenko, A. B. Kramers−Kronig Constrained Variational Analysis of Optical Spectra. *Rev. Sci. Instrum.* **2005**, *76* (8), No. 083108.

https://dx.doi.org/10.1021/acsanm.0c03221
ACS Appl. Nano Mater. 2021, 4, 2351−2356